PAPER

Experimental signatures of direct-laser-acceleration-assisted laser wakefield acceleration

IOP Publishing Plasma Physics and Controlled Fusion
Plasma Phys. Control. Fusion **60** (2018) 044012 (10pp) https://doi.org/10.1088/1361-6587/aaade1

Experimental signatures of direct-laser-acceleration-assisted laser wakefield acceleration

J L Shaw[1,2], N Lemos[2,3], K A Marsh[2], D H Froula[1] and C Joshi[2]

[1] Laboratory for Laser Energetics, University of Rochester, 250 E River Rd, Rochester, NY 14623, United States of America
[2] Department of Electrical Engineering, University of California Los Angeles, 405 Hilgard Ave, Los Angeles, CA 90095, United States of America
[3] Lawrence Livermore National Laboratory, 7000 East Avenue, Livermore, CA 94550, United States of America

E-mail: jshaw05@lle.rochester.edu

Received 29 November 2017, revised 1 February 2018
Accepted for publication 8 February 2018
Published 28 February 2018

Abstract

The direct laser acceleration (DLA) of electrons in a laser wakefield accelerator (LWFA) operating in the forced or quasi-blowout regimes has been investigated through experiment and simulation. When there is a significant overlap between the trapped electrons and the drive laser in a LWFA cavity, the resulting electrons can gain energy from both the LWFA and the DLA mechanisms. Experimental work investigates the properties of the electron beams produced in a LWFA with ionization injection by dispersing those beams in the direction perpendicular to the laser polarization. These electron beams show certain spectral features that are characteristic of DLA. These characteristic features are reproduced using particle-in-cell simulations, where particle tracking was used to elucidate the roles of LWFA and DLA to the energy gain of the electrons in this experimental regime and to demonstrate that such spectral features are definitive signatures of the presence of DLA in LWFA.

Keywords: laser wakefield acceleration, direct laser acceleration, laser plasma accelerator

(Some figures may appear in colour only in the online journal)

Introduction

As the field of laser wakefield acceleration (LWFA) [1] matures, emphasis is shifting toward utilizing LWFA as a source of electron beams and x-rays for applications. There is an increasing emphasis on producing electron beams from LWFAs that can meet the stringent beam requirements (narrow divergence, small emittance, narrow energy spread) necessary for use in staged plasma accelerators [2] and free electron lasers. Simultaneously, betatron x-rays from LWFA are being utilized for applications [3–7], which places an emphasis on optimizing LWFA to produce these x-rays. Even though these applications require optimization of different electron beam properties, all applications benefit from a more-complete understanding of the dynamics of electron energy gain in LWFA and how those dynamics affect properties such as electron beam energy, divergence, source size, shape, and energy spread.

For the range of plasma densities (mid-10^{18} to a few 10^{19} cm^{-3}) and laser pulse durations (35–45 femtoseconds full width at half maximum) that are typically used in many current LWFA experiments in the forced or quasi-blowout regimes, the laser pulse length is on the order of the wake wavelength; therefore it may occupy the entire first bucket of the wake. In such experiments, the wakefield structure has a desirable transverse and longitudinal field structure for generating a self-injected electron bunch, but it also has the conditions needed for direct laser acceleration (DLA) [8, 9] if there is an overlap between the accelerating electrons and the transverse electric field of the laser pulse [10–16]. It is therefore important to understand the role that not only the longitudinal electric field of the wake, but also the other fields

—namely, the transverse fields of the ion column and of the laser itself—play in determining the ultimate energy gained by the electrons. In this paper, we show through experiments direct, observable signatures in the produced electron beams that indicate that DLA makes a significant contribution to the electrons' energy in LWFAs operated in such a configuration. Three-dimensional (3D) particle-in-cell (PIC) simulations are used to elucidate the energy dynamics that lead to this contribution.

Background

In the matched, self-guided [17] blowout regime of LWFA [18], an ultrashort, intense laser pulse propagates through either an underdense plasma or a neutral gas. In the latter case, the leading edge of the laser pulse ionizes the neutral gas, and the pondermotive force of the laser then expels the plasma electrons out and around the main body of the pulse. On the femtosecond (fs) timescale of the laser, the more-massive ions remain relatively immobile, so an ion column forms behind the drive laser. The Coulomb force of that ion column pulls those expelled plasma electrons back to the laser axis, where they overshoot the axis and establish a wake oscillation. The charge separation generated by this wake structure produces a longitudinal electric field that is capable of accelerating electrons trapped in the wake at gradients >1 GeV cm^{-1}. Electrons that are trapped off-axis will execute betatron oscillations due to the linear transverse focusing force of the ion column [19, 20].

Electrons can become trapped in a LWFA by a variety of methods [21–31], but in the experiments and simulations presented here, the ionization injection [32–34] technique is used. In this technique, the plasma is produced by the laser ionization of a neutral gas mixture comprised of a gas with a low ionization potential (commonly He or H_2) doped with a gas with high ionization potential (commonly N_2 or Ar). The lower-intensity front edge of the laser pulse ionizes the outer (typically L) shell electrons of the dopant gas along with all the electrons in the gas with a low ionization potential. Because the inner (typically K) shell electrons of the higher-Z atoms have a much higher ionization potential, they are ionized only near the peak of the laser pulse within a fully formed wake and are subsequently trapped without slipping all the way to the back of the wake. Compared to self-trapping, this method of ionization injection permits trapping in a LWFA at reduced plasma densities and laser powers.

In a LWFA operating in the forced or quasi-blowout regime, the ion column acts as a very strong wiggler. Trapped electrons that are being accelerated by the wake undergo betatron oscillations in response to the transverse electric field of the ion column. Therefore, if a LWFA is configured such that some of the trapped electrons undergo betatron oscillations in the polarization plane of the laser's electric field, the transverse field of the drive laser can give the electrons additional transverse momentum. This transverse momentum can then be converted into longitudinal momentum through the $\mathbf{v} \times \mathbf{B}$ force of the laser. Thus, the DLA mechanism [8, 9] can accelerate electrons by this coupling of the transverse field of the laser through the betatron motion of the electrons. As a result, there is a potential for those electrons to be accelerated by the DLA mechanisms in addition to the LWFA mechanism in a LWFA where the drive laser overlaps the trapped electrons [10–16].

It has been noted that DLA is the inverse of the ion channel laser mechanism [35]. DLA in LWFA is also similar to inverse free electron laser (IFEL) acceleration [36, 37], except that the static magnetic undulator used in an IFEL is replaced by the transverse electric field of the ions in DLA and the resonance condition need not be strictly obeyed as in the IFEL [11, 13, 14]. In principle, the resonance condition for DLA is similar to that for an IFEL [38]; i.e., in an ideal situation, the laser pulse overtakes the electrons by one wavelength per betatron oscillation once the electrons come into resonance with the fundamental ($N = 1$) harmonic, where the electrons are bunched on a laser-wavelength scale [8, 39–42]. However, unlike in an IFEL, sustained resonance for DLA is more difficult to design because in the latter case, the normalized undulator strength $K \gg 1$ and the energy and betatron frequency of the electrons as well as the laser properties are continuously and rapidly changing [11, 13, 14].

The condition for energy gain from the DLA mechanism is typically expressed using the one-dimensional resonance condition for a single electron [8, 9]

$$N\omega_\beta = (1 - v_\parallel/v_\phi)\omega_0, \tag{1}$$

where N is an integer indicating the harmonic of the betatron frequency

$$\omega_\beta = \frac{\omega_p}{\sqrt{2\gamma}}. \tag{2}$$

$v_\parallel$ is the velocity of the electron in the longitudinal direction, and v_ϕ and ω_0 are the phase velocity and frequency, respectively, of the electromagnetic wave (i.e., laser). Essentially, this resonance condition means that in order for an electron to gain energy from DLA, a harmonic of the betatron frequency $N\omega_\beta$ must equal the Doppler-shifted laser frequency $(1 - v_\parallel/v_\phi)\omega_0$ witnessed by the electron [8, 9, 11, 13, 14]. It is well known that in LWFAs, especially those not in the ideal blowout regime [18], the properties of the drive laser, including ω_0 and v_ϕ, evolve throughout the acceleration distance. Furthermore, as electrons are accelerated in a LWFA, their longitudinal momentum, and therefore $v_\parallel$, increases, and their betatron frequency is expected to fall as $\gamma^{-1/2}$ as seen in equation (2). Despite these evolving quantities, electrons that are being accelerated in a LWFA are able to gain significant energy from DLA because the quantities evolve together such that a quasi-resonance is set up and the electrons are in a phase where they gain energy from the DLA mechanism for more than one-half of each betatron cycle [11, 13, 14].

To determine if a LWFA is operating in a regime where DLA is expected to contribute to the energy gain of the electrons, the LWFA can be characterized using the ratio of the laser pulse length τ_{laser} to the nonlinear plasma wavelength Λ_{wake}. This ratio can be expressed as a dimensionless

pulse length parameter [13, 14]

$$T_p = c\tau_{laser}/\Lambda_{wake} = \omega_p \tau_{laser}/(2\pi a_0{}^{1/2}). \quad (3)$$

If the laser pulse length $c\tau_{laser}$ equals the a_0-dependent length of the first period of the wake [18] $\Lambda_{wake} \simeq \sqrt{a_0}\frac{2\pi}{k_p}$, then $T_p = 1$. Here, $k_p = \omega_p/c$, and a_0 is the normalized vector potential $a_0 = eE_0/mc\omega_0 \simeq 8.6 \times 10^{-10}\sqrt{I_0\ (\mathrm{W\ cm^{-2}})}\ \lambda\ (\mu\mathrm{m})$, where I_0 is the laser intensity and λ is the wavelength of the laser. In the case where T_p is 0.5 or less, the laser does not overlap the trapped electrons in the LWFA while they are being accelerated; those electrons gain energy purely from the longitudinal wakefield [10, 13, 14]. When T_p reaches 0.6 or more, the laser pulse will overlap the trapped electrons, and DLA can play a role in the acceleration of those electrons [10, 13, 14]. When the value of T_p exceeds 1, there is a substantial overlap between the transverse laser field and the trapped electrons [13, 14].

Experimental methods and results

In this section, we show definitive experimental evidence of the presence of DLA in nonlinear LWFAs where the laser pulse overlaps the trapped electrons. We first demonstrate that the electron beams are indeed interacting with the drive laser when there is an overlap between the laser and trapped electrons, as might be expected in a DLA-assisted LWFA experiment. We then show that the transverse structure of the dispersed electron beams exhibits characteristic features that are indicative of DLA as an additional acceleration mechanism.

The experiments presented in this paper were conducted at UCLA using a Ti:Sapphire laser with a central wavelength of 815 nm and a fixed τ_{laser} of 45 ± 5 fs full width at half maximum of intensity. The laser was run with powers P up to 10 TW, which correspond to an a_0 up to 2.6. An $f/6$ off-axis parabola (OAP) system focused the laser pulse to a spot size w_0 of 6.7 μm at the entrance of a variable-length (0.1–2 mm) gas cell [43, 44] as shown in figure 1. The gas cell was filled with a 95% He/5% N_2 neutral gas mixture using a pulsed solenoid valve. The gas mixture was utilized so that ionization injection [32] could be used to both inject charge early into the wake and increase the amount of trapped charge. The plasma density was controlled by changing the gas pressure and was measured on each shot using a Michelson interferometer [43, 44]. The produced electron beams were dispersed in energy with a 0.92 tesla (T) dipole magnet onto a plastic scintillator or a LANEX screen. Images were collected using a PI-MAX intensified CCD camera. This electron spectrometer could be rotated by 90° so that the electron beam could be dispersed parallel to or orthogonal to the linear laser polarization [13, 14].

Because the energy gain from DLA relies on the coupling between the transverse laser field and the betatron motion of the electrons, the first observable signature of an interaction between the laser and the trapped electrons in a LWFA is that the undispersed electron beam should be elliptical in the direction of the laser polarization [45]. The white ellipses in figure 2(a) are fits to the 50% contour of the undispersed

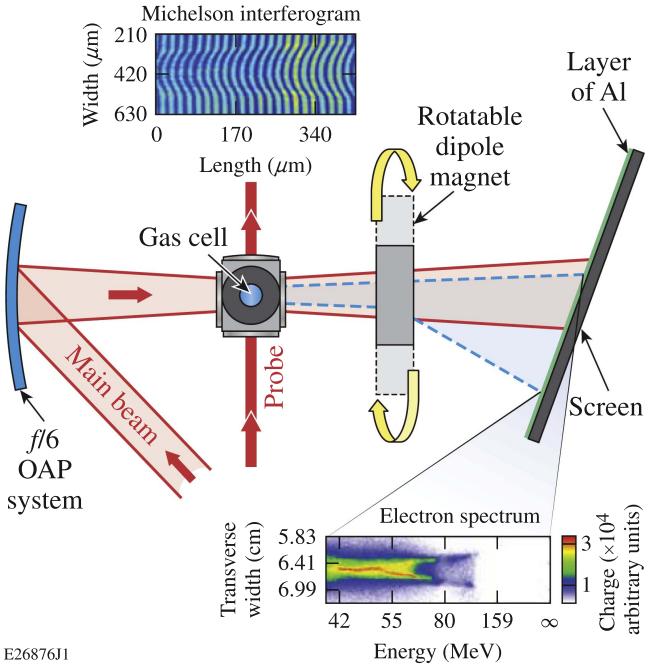

Figure 1. Experimental setup. The thick red line shows the main laser pulse being focused by the $f/6$ OAP system at the entrance of the gas cell. The laser is linearly polarized in the plane of the page. The thin red line shows the probe for the Michelson interferometer. A typical interferogram is shown. The electrons are dispersed by the 0.92 T dipole magnet onto a scintillator or a LANEX and imaged by a PI-MAX 3 camera. The dipole magnet and screen could be rotated by 90° so that the electron beams could be dispersed parallel or orthogonal to the laser polarization. The dipole magnet typically was located 3.2 cm downstream from the gas cell, and the distance from the end of the magnet to the screen was 7.0 cm. A typical measured electron spectrum is shown.

electron beams from 10 consecutive shots where the laser had horizontal, linear polarization and a vacuum a_0 of ~1.5. The plasma density was ~$1.7 \times 10^{19}\ \mathrm{cm^{-3}}$, which yields a T_p value of ~1.3, and the gas cell length was 900 μm. The fits show a strong ellipticity in the direction of the laser polarization with an average measured half-width at half-maximum (HWHM) divergence of 12.2 mrad. In contrast, the average measured HWHM divergence in the perpendicular direction was 5.6 mrad. The direction of the linear polarization of the drive laser was then rotated 90° using a thin (1 mm) quartz half wave plate for high-laser-energy applications. The ellipticity of the undispersed electron beams rotated with the laser polarization, as shown in figure 2(b), which indicates that the trapped electrons' transverse momentum is being enhanced in the polarization plane. With the vertical laser polarization, the average measured HWHM divergence in the direction of the laser polarization was 13.0 mrad, and the average measured HWHM divergence in the perpendicular direction was 6.5 mrad. Therefore, under the laser-plasma parameters described above, the measured divergence of undispersed electron beams emanating from the LWFA shows ellipticity that is correlated to the polarization of the laser pulse. This correlation demonstrates that the electrons are indeed interacting with the drive laser. Although DLA is expected to preferentially increase the divergence of the

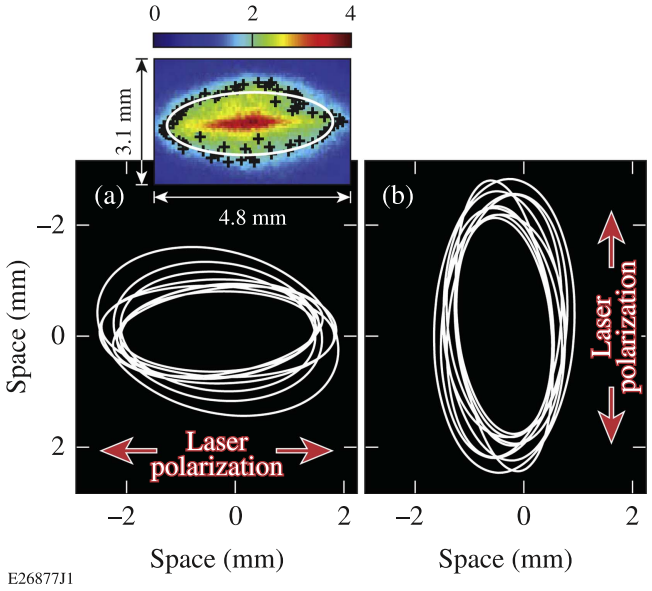

Figure 2. (a), (b) Fits (white ellipses) to the 50% contour of undispersed electron beams from a series of 9 and 10, respectively, consecutive laser shots when using horizontal and vertical, respectively, linear laser polarization. (Inset) Typical undispersed electron beam from data shown in (a) with 50% contour points marked by the black crosses and the fit to that point marked by the white ellipse.

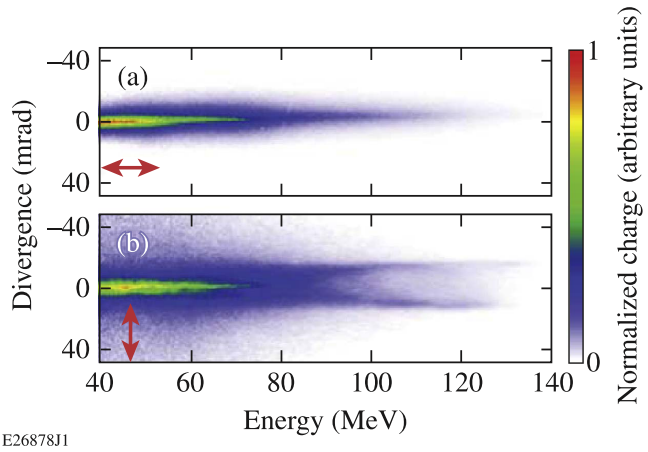

Figure 3. (a) Experimental electron spectrum dispersed parallel to the laser polarization (red arrow) for a gas cell length = 800 μm, $n_e = 1.7 \times 10^{19}$ cm^{-3}, $a_0 = 2.0$, and $T_p = 1.1$. (b) Experimental electron spectrum dispersed perpendicular to the laser polarization (red arrow) for a gas cell length = 900 μm, $n_e = 1.4 \times 10^{19}$ cm^{-3}, $a_0 = 1.9$, and $T_p = 1.1$.

electron beam in the plane of the laser polarization, the observed ellipticity in the divergence of the undispersed electron beams in figure 2 in itself is not definitive proof that DLA is present in the LWFA [13]. Rather, a signature of the increased transverse momentum must be present in the energy gain of the electrons to demonstrate the presence of DLA in LWFA.

Because DLA is an additional energy gain mechanism on top of the energy gained from the wakefield, if it is present in the system, the highest-energy electrons should also have the largest divergence. Figure 3 compares two electron spectra that were taken for comparable experimental parameters. The spectrum in figure 3(a) shows the electron beam after it was dispersed in the same direction as the laser polarization. In the transverse dimension, this spectrum is peaked on-axis. It has an average measured HWHM divergence of 4.3 mrad for the electron energies shown. For figure 3(b), the electron spectrometer was rotated by 90° so that the electron beam was dispersed orthogonal to the direction of the laser polarization. In the transverse dimension, the shape of this spectrum is very different than then spectrum shown in figure 3(a), where the electron beam was dispersed in the same direction as the laser polarization. This spectrum has a larger divergence and clearly splits into a forked structure for electron energies above 90 MeV. The average divergence of this spectrum was 11.8 mrad and was found using the HWHM for electrons with final energies <90 MeV and the fork centroid for electrons with final energies >90 MeV, which is where the fork structure begins. Such clear fork structures, partial fork structures, or modulations have been observed in experimental electron spectra for plasma densities between (0.9–1.6) $\times 10^{19}$ cm^{-3} ($T_p = 0.8$–1.4) as shown in figure 4. The electrons that comprise the charge that is peaked on-axis gain the bulk of their energy from LWFA. They are accelerated either in the first bucket of the wakefield but in a region that does not overlap the drive laser or in later buckets. Those electrons that comprise the fork are accelerated in the first bucket of the wake and gain energy from both the DLA and the LWFA mechanisms, as will be shown in the Simulation section.

Simulation methods and results

To interpret the features observed in experiment, a series of 3D simulations using the PIC code OSIRIS 3.0 [46] were conducted. These simulations modeled the above experimental parameters and utilized particle tracking to determine the relative contribution of LWFA and DLA to the total energy gain of the electrons in this regime. The spectral features indicating if DLA is present in a LWFA are best illustrated by comparing a simulation where T_p is 0.4 (no overlap between the laser and the trapped electrons) and a case where T_p is 0.8 (drive laser is filling nearly the entire first period of the wake and overlapping the trapped electrons). DLA is expected in the $T_p = 0.8$ case [10, 13, 14]. Both simulations were run with identical parameters except for the laser pulse lengths. The laser ionized a 99.9%He/0.1%N_2 neutral gas mixture to produce a plasma with a density of 8×10^{18} cm^{-3}. The Ammosov–Delone–Krainov [47] ionization model was used. The resulting plasma consisted of 1 mm-long plateau region with 100 μm-long linear density up and downramps. The linearly polarized drive laser had an a_0 of 2.1 and was focused to a spot size of 6.7 μm halfway up the density upramp. For the $T_p = 0.4$ case, the pulse length was 25 fs; for the $T_p = 0.8$ case, the pulse length was 45 fs. For both simulations, the grid was 1940 × 320 × 320 with 2 × 2 × 2 particles per cell and $k_0\Delta z = 0.209$ and $k_p\Delta x$, $\Delta y = 0.090$. The resulting normalized time step was 0.014 03.

Each simulation was run once to completion, and then the 20 highest-energy electrons and >500 random electrons

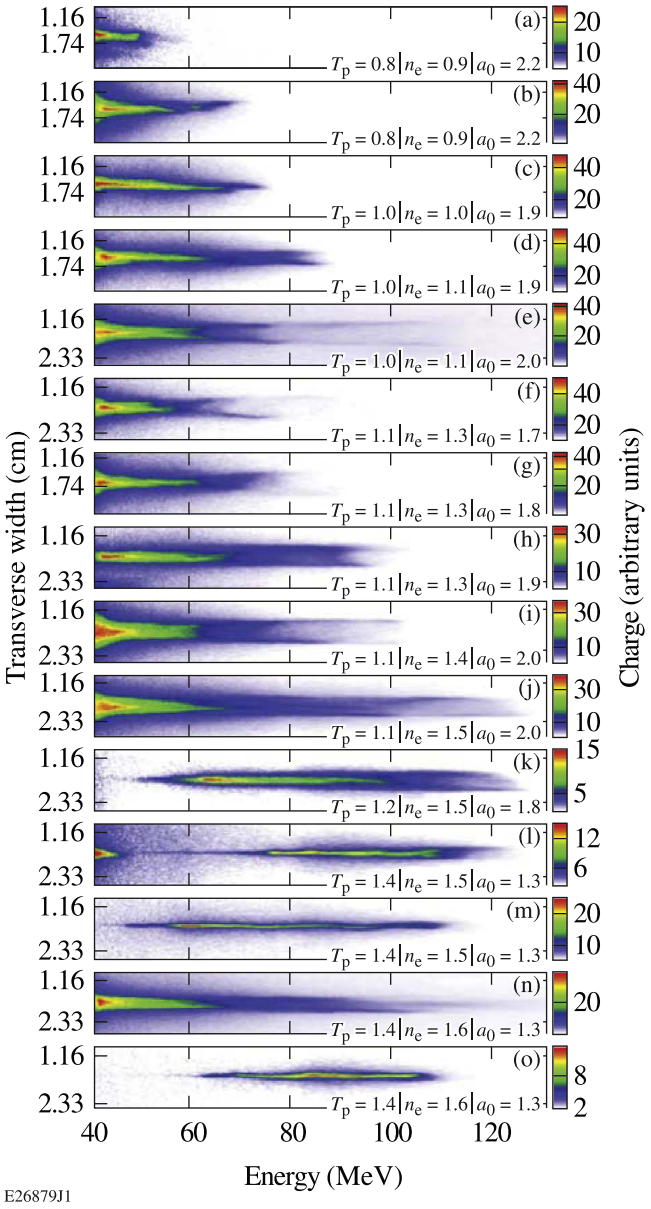

Figure 4. Series of electron spectra with fork features or modulated spectra taken on a single shot day. Data is sorted by ascending T_p values. Gas cell length was 900 μm. At the highest densities of (1.5–1.6) $\times$ 10^{19} cm^{-3}, even though $T_p > 1$, the fork structure disappears as a_0 is reduced to 1.3 thereby switching off ionization injection.

were tagged. The simulations were then rerun while tracking the tagged particles to determine their position, momentum, and the fields that they sampled at each time step of the simulation. With that information, the relative contributions to the total energy gain of each electron due to the transverse electric field and the longitudinal electric field can be calculated. The relative contribution $W_{||}$ due to the longitudinal electric field $\mathbf{E}_{||}$ was calculated using

$$W_{||} = -e\int_0^t \mathbf{E}_{||} \cdot \mathbf{v}_{||} \mathrm{d}t'. \quad (4)$$

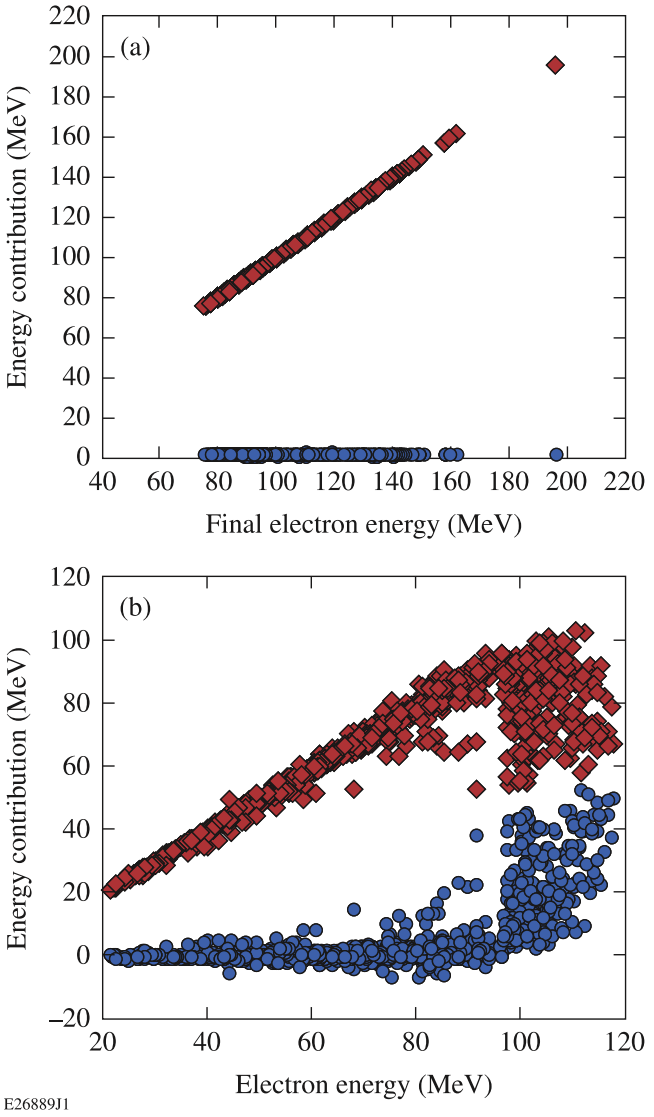

Figure 5. DLA contribution $W_\perp$ (blue circles) and LWFA contribution $W||$ (red diamonds) to the total electron energy of (a) the 550 random electrons in the $T_p = 0.4$ case and (b) the 1080 random electrons in the $T_p = 0.8$ case.

The dominant longitudinal electric field is the wakefield; therefore, this value will be called the 'LWFA contribution' to the final electron energy. Similarly, the relative contribution $W_\perp$ due to the transverse electric field $\mathbf{E}_\perp$ was calculated using

$$W_\perp = -e\int_0^t \mathbf{E}_\perp \cdot \mathbf{v}_\perp \mathrm{d}t', \quad (5)$$

where $\mathbf{v}_\perp$ is the transverse velocity of the electron. The dominant transverse electric field is the transverse laser field, so this value will be called the 'DLA contribution' to the final electron energy.

In the $T_p = 0.4$ case, LWFA is expected to be the only acceleration mechanism. Figure 5(a) shows that indeed DLA plays a negligible role in the energy gained by the electrons when there is no overlap between the laser and the trapped electrons. Of the 550 randomly selected electrons, the

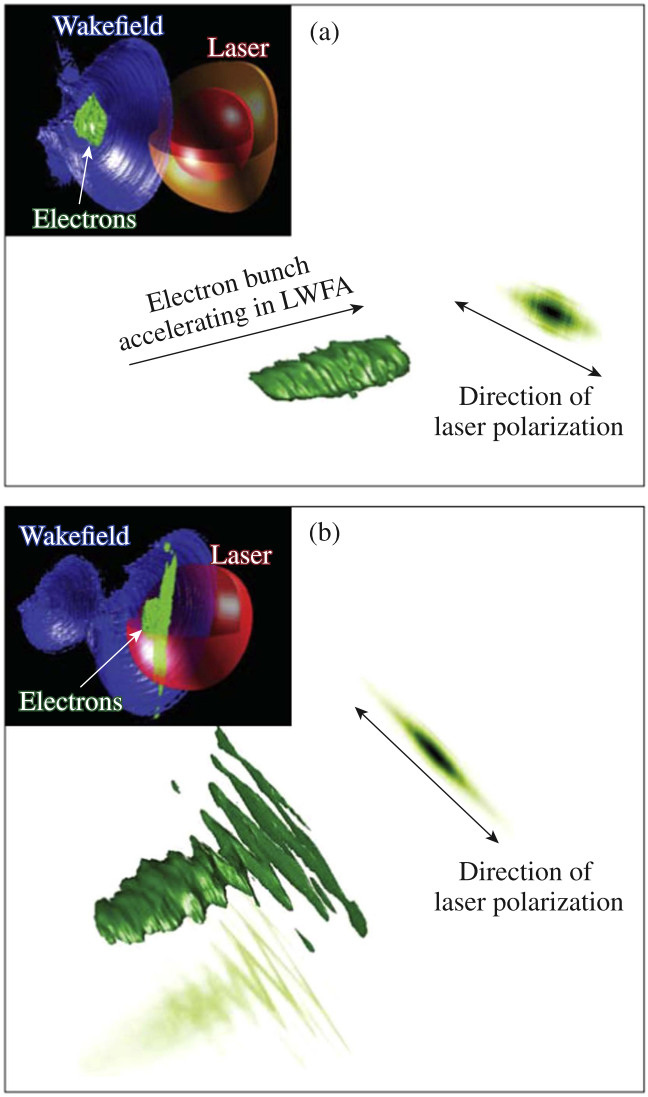

Figure 6. Contour plot of electron bunch (green) propagating in a 3D OSIRIS simulation (left) and projection of that electron bunch onto a screen (right) for (a) the $T_p = 0.4$ simulation and (b) a $T_p = 0.8$ simulation. Insets show snapshots of the electron bunch as it is accelerated in the LWFA. Note that the laser overlaps the trapped electrons in the $T_p = 0.8$ case.

maximum DLA contribution as calculated using equation (5) is 1.5 MeV, and DLA accounts for no more than 1.5% of the final energy of any of the randomly tagged electrons. In the $T_p = 0.8$ case, the drive laser now overlaps the trapped electrons and some contribution from DLA is expected in addition to LWFA. Figure 5(b) shows that although the maximum electron energy is reduced, DLA plays a significant role in the energy gained by the electrons. For the 1080 randomly selected electrons, the maximum DLA contribution to the final electron energy is up to 50 MeV, and up to ~50% of the electrons' total energy can be attributed to DLA, which shows that the DLA mechanism can provide comparable energy to the LWFA mechanism.

If DLA contributes significantly to the energy gain of the electrons produced from a LWFA, then those electrons should have increased transverse momentum in the direction of the laser polarization. This increased transverse momentum should show up as an ellipticity of the produced electron beam in the direction of the laser polarization. Figure 6 compares the projected divergence for the $T_p = 0.4$ and the $T_p = 0.8$ cases. In the $T_p = 0.4$ case, the inner-shell nitrogen electrons were ionized within the laser pulse and then escaped the laser to become trapped in the back of the wake, which causes the initial transverse momentum that they gain from the laser [13] to become apparent. In this case, the projection of the accelerated electrons on a screen (figure 6(a)) shows an elliptical beam with an RMS divergence of 8.6 mrad along the major axis, which is in close agreement with estimations of the maximum transverse momentum an electron acquires from the tunnel ionization process [13]. In the case of $T_p = 0.8$, the ionized electrons remain within the laser field and gain energy from both LWFA and DLA. These electrons also show an elliptical beam when projected onto a screen (figure 6(b)). Its RMS divergence along the major axis is 24.8 mrad, which is nearly 3× as large as in the $T_p = 0.4$ case, where LWFA is the only acceleration mechanism. Although both simulations produce an elliptical beam, the observation of increased divergence in the $T_p = 0.8$ case is qualitatively consistent with expectations if DLA is present as an additional acceleration mechanism.

If LWFA is the only acceleration mechanism, the divergence of the produced electron beam should be relatively constant as a function of energy regardless of the direction of the dispersion of the electron beam. Figure 7(a) shows the electrons dispersed in the direction of the laser polarization for the $T_p = 0.4$ case. The resulting electron spectrum has a narrow divergence that is peaked on-axis. When the electrons are dispersed orthogonal to the laser polarization (figure 7(b)), the divergence remains relatively narrow and is still peaked on-axis. Such narrow divergence is consistent with LWFA being the only acceleration mechanisms. To further illustrate this point, in figure 7(c), the 550 randomly tagged electrons color coded by their energy gain from DLA are plotted on a contour plot of figure 7(b). This figure shows that the maximum DLA contribution is only 1.5 MeV, and there is no correlation between the amount of energy contributed by DLA and the divergence of the electron beam.

DLA arises due to an increase in the transverse momentum of the electron caused by work done by the transverse laser field. Because DLA is an additional energy gain mechanism on top of the energy gained from the wakefield, if it is present in the system, the highest-energy electrons should also have the largest divergence. Nonetheless, as figure 7(d) shows, even in the $T_p = 0.8$ case where DLA is expected to contribute to the energy gain, if the electrons are dispersed in the direction of the laser polarization, the spectrum still features a narrow divergence that is peaked on axis. If the electron beam is dispersed in the same direction of the laser polarization, any features associated with the large-radii betatron oscillations of the electrons in the direction of the laser polarization cannot be detected. However, when the electron beam is dispersed orthogonal to the direction of the laser polarization, figure 7(e) shows that the divergence increases with the total energy of the electrons,

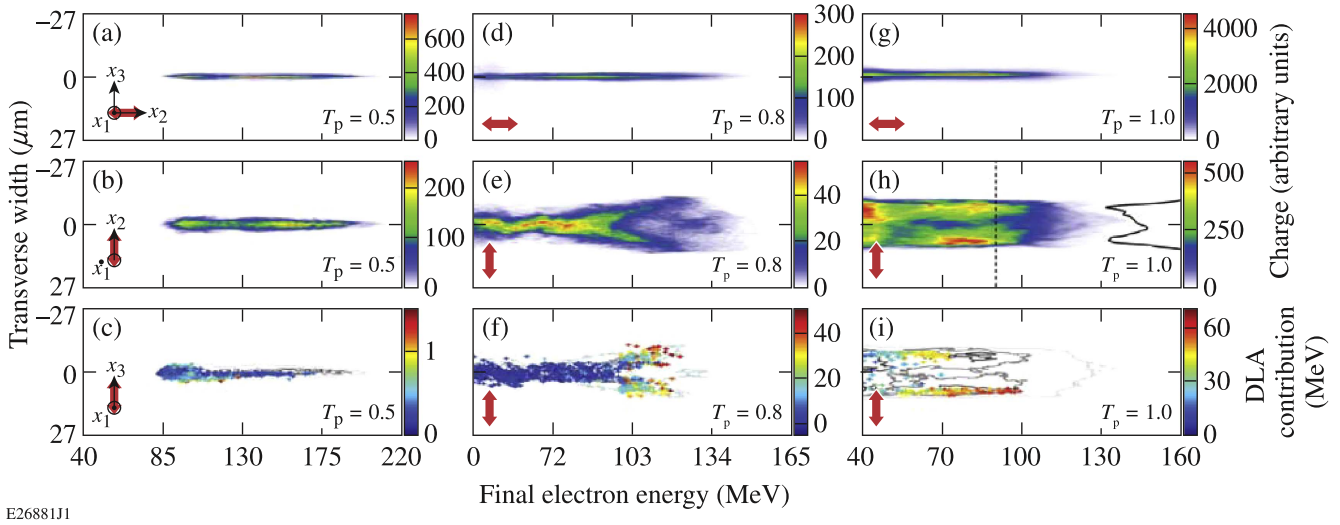

Figure 7. Electron spectra from OSIRIS simulations with T_p values of (a)–(c) 0.4, (d)–(f) 0.8, and (g)–(i) 1. Parameters for the $T_p = 1$ simulation were: $a_0 = 2.03$, $\tau_{laser} = 45$ fs, $\lambda_0 = 815$ nm, $w_0 = 6.7$ μm, $n_e = 1.43 \times 10^{19}$ cm^{-3}, plasma length = 430 μm with 100 μm up- and 150 μm downramps. The grid was 1814 × 320 × 320 with 2 × 2 × 2 particles per cell and $k_0\Delta z = 0.209$ and $k_p\Delta x$, $\Delta y = 0.120$. The resulting normalized time step was 0.018 77. (a), (d) and (g) Electron spectra dispersed parallel to the laser polarization (red arrow) for T_p of 0.4, 0.8, and 1, respectively. (b), (e), and (h) Electron spectra dispersed perpendicular to the laser polarization (red arrow) for T_p of 0.4, 0.8, and 1, respectively. The black line in (h) represents the lineout (dashed line) of the forked structure at 90 MeV. (c) Contour plot of (b) where the light gray, dark gray, and black lines represent the 8%, 40% and 60% contours. The colored crosses show the 550 randomly tagged electrons with final energies above 40 MeV colored by their DLA contribution. (f) Contour plot of (e) where the light gray, dark gray, and black lines represent the 18%, 44%, and 74% contours. The colored crosses show the 1080 randomly tagged electrons with final energies above 40 MeV colored by their DLA contribution. (i) Contour plot of (h) where the light gray, dark gray, and black lines represent the 4%, 35%, and 61% contours. The colored crosses show the 550 randomly tagged electrons with final energies above 40 MeV colored by their DLA contribution.

and at an energy of ∼95 MeV, that the spectrum splits into a forked structure. In figure 7(f), the 1080 random electrons are superimposed on a contour plot of the data shown in figure 7(e). The color of these electrons indicates the DLA contribution to their final energies. Figure 7(e) shows that for final electron energies below ∼95 MeV, where the transverse shape of the electron spectrum is peaked on-axis, the DLA contribution to the final electron energies is small (15 MeV or less). Rather, the center-peaked charge at lower energies, which was also seen in the experimental data in figure 3(b), is predominately accelerated by the wake. Beginning at final electron energies ∼95 MeV, the DLA contribution to the electron energy increases, and the electron spectrum splits into a forked structure similar to the one seen in the experimental data (figure 3(b)). The electrons in the fork have the largest DLA contributions, and thus the change in transverse width with energy is a clear, observable signature that DLA is playing a role in the LWFA.

The degree of forking seen in the electron spectrum depends on the degree of overlap between the drive laser and the trapped electrons. The electron spectrum in figure 7(h) was produced from a 3D OSIRIS simulation that had the same physical parameters as the $T_p = 0.8$ simulation, except that a_0 was 2.03, n_e was 1.43×10^{19} cm^{-3}, and the constant-density region of the plasma was 430 μm long. These parameters were chosen to model the experimental data shown in figure 3. Comparing the middle row of spectra in figure 7 shows that as the degree of overlap (i.e., T_p) is increased from $T_p = 0.5$ to $T_p = 1.0$, the extent of the forking increases and the forking descends deeper into the lower-energy portion of the electron spectrum. The increase in forking with T_p is caused by an increase in the DLA contribution relative to the LWFA contribution. As shown in figure 5, for the $T_p = 0.8$ case, the dominant energy contribution for the randomly selected electrons is from LWFA. Up until final electron energies of ∼95 MeV, it is essentially the only mechanism contributing to the energy gain of the electrons; indeed, there is no forking of the electron spectrum (figure 7(e)) below these energies. The fork structure arises when DLA begins to make a sizeable contribution. At energies of ∼95 MeV, DLA begins to contribute to the final energy gained by the electrons; it is at that energy that the spectrum begins to fork (figures 7(e) and (f)). In comparison to the $T_p = 0.8$ case, for the 550 randomly selected electrons from the $T_p = 1.0$ case, even the lowest electron energies have significant energy contributions from DLA, and both DLA and LWFA are strongly contributing to the energy gain of the electrons as seen in figure 8. The best linear fits through those contributions show that the curves intersect at 25 MeV. Below this energy, the final energy of the electrons is primarily dominated by LWFA, and above this energy, DLA becomes the dominant contribution and indeed, this is correlated with the strong forking observed in figures 7(h) and (i) [13, 14].

An examination of the transverse profile of the accelerating electron beam reveals the source of the forked structure. When DLA is present in a LWFA, the higher-energy electrons gain significant energy from DLA. The head of the electron beam overlaps a high-intensity portion of the laser

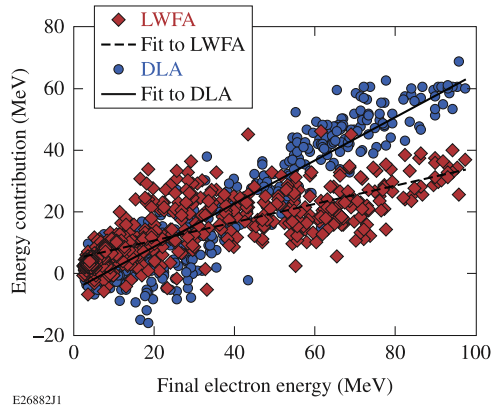

Figure 8. DLA contribution $W_{\perp}$ (blue circles) and LWFA contribution $W_{||}$ (red diamonds) to the total electron energy for the 550 random electrons in the $T_p = 1$ case. The solid black line represents the best linear fit to the DLA contribution ($E_{DLA} = 0.70$ $E_{final} - 5.36$ (MeV) with an R^2 fit of 0.88). The dashed black line represents the best linear fit to the LWFA contribution ($E_{DLA} = 0.30$ $E_{final} + 4.77$ (MeV) with an R^2 fit of 0.57).

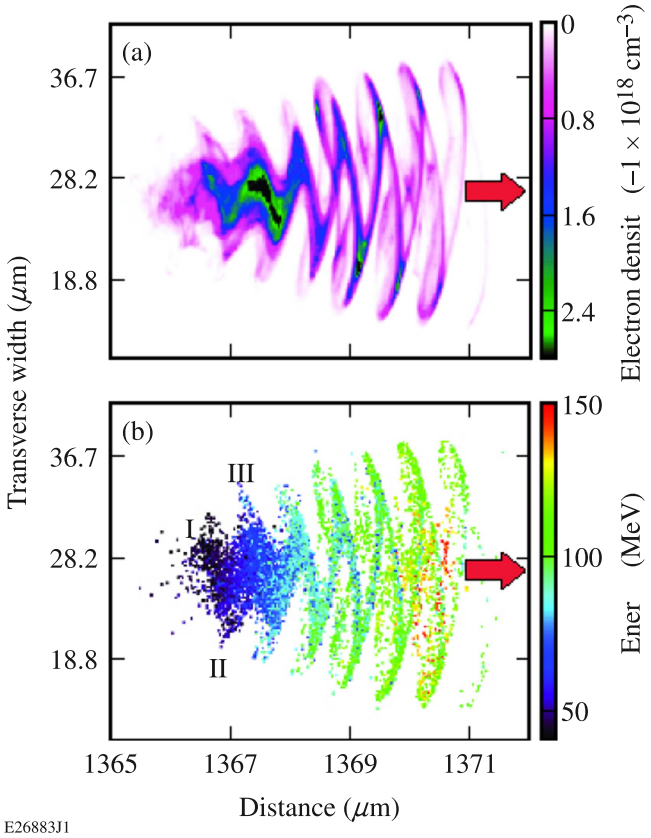

Figure 9. (a) Transverse density profile of electron beam after propagating 100 μm in vacuum from the $T_p = 0.8$ simulation used to generate figures 7(e) and (f). (b) Transverse profile of the same electron beam as in (a) showing a sampling of 0.04% of the total electrons in the simulation color coded by their final energy. The red arrows in both (a) and (b) mark the direction of the electron beam propagation.

pulse and is strongly modulated at the half-laser wavelength [48], and the charge is bunched at the extrema of the betatron oscillations as shown in figure 9(a). This bunching causes the charge at the front portion of the electron beam to exit the plasma with some transverse separation, which leads to the fork structure seen in the middle and bottom rows of figure 7. The laser intensity falls from the head of the electron beam to its tail; consequently, the modulation at the half-laser wavelength becomes less pronounced and the charge is no longer bunched at the extrema of the betatron oscillations. At the tail of the electron beam, the energy contribution of DLA to the overall charge of the electrons is small, and there is only a small transverse modulation of the accelerated charge. Although this transverse modulation is small at the tail of the beam, it leads to the serpentine structure in the dispersed electron beam in the $T_p = 0.8$ case (figure 7(e)) for the lower electron energies (40–95 MeV).

In figure 9(b), the transverse structure of the electron beam is shown using a sampling of the electrons from the $T_p = 0.8$ simulation color-coded by their final energy. Figure 9(b) shows that there is a general correlation between the position of the electrons in the beam and their final energies. The higher-energy electrons are predominantly found at the head of the electron beam, and the lower-energy electrons are predominantly found at the tail. For the lower-energy electrons, each half oscillation in the transverse structure contains electrons in different bins of final energies. For example, the charge slightly above the laser axis at the point marked 'I' has final energies ~40 MeV, the charge at 'II' has ~50 MeV, the charge at 'III' has ~70 MeV and so on. These steps in the final energy associated with a given transverse position mean that the different-energy electrons will exit the plasma with slightly different transverse positions and divergences, which produces the serpentine structure when the electron beam is dispersed orthogonal to the direction of the laser polarization as seen in the center-peaked electron feature for energies from 40 to ~95 MeV in figure 7(e). This serpentine structure is absent when the electron beam is dispersed in the direction of the laser polarization as seen in figure 7(d).

In addition to the serpentine structure in the dispersed spectrum for electron energies below ~95 MeV, figures 7(e) and (f) have a second small forked structure in the interior of the large fork at an energy of approximately 125 MeV. As already discussed, the main fork structure in figure 7 arises because the electrons are bunched at the extrema of their betatron oscillation and exit the plasma with a transverse separation but a small divergence. The secondary fork in figure 7 also arises due to the betatron motion of the electrons; however, this fork is formed differently. The electrons that form this fork are also executing large-radii betatron oscillations. However, they are phased one quarter of a betatron period from those that form the main fork. Therefore, unlike the electrons that form the main fork, which exit the plasma with a large transverse separation but small divergence, these electrons exit the plasma with a small transverse separation but with a large divergence. Because the electron beam spectrum from the simulation is calculated 100 μm after the exit of the plasma, these electrons are captured as they cross the betatron axis due to their large divergence. Such electrons would not be captured in the experiment however because their divergence is so large that they would be lost during the transport to the detector.

Conclusions

In this paper, the DLA of electrons in a LWFA operating in the forced or quasi-blowout regimes has been investigated through experiment and simulation. We have demonstrated that when there is a significant overlap between the trapped electrons and the laser ($T_p \sim 1$) in a LWFA, the accelerated electrons can gain significant energy from both LWFA and DLA. In the experimental work, we investigated the properties of the electron beams produced in a LWFA with ionization injection by dispersing those beams in the direction perpendicular to the laser polarization. We found that these electron beams show certain features (ellipticity in the plane of the laser polarization and an energy spectrum that splits into a fork at higher energies when the beam is dispersed orthogonal to the laser polarization direction) that are characteristic of DLA. These characteristic spectral features were reproduced in OSIRIS simulations, where particle tracking was used to demonstrate that such spectral features are signatures of the presence of DLA in LWFA.

Supporting simulations modeled the experimental parameters and employed particle tracking to interpret these signatures and elucidate the roles of LWFA and DLA to the energy gain of the electrons in this experimental regime. The contribution of DLA to the energy gained by the electrons was calculated in simulations. Its magnitude was found to be on the order of the LWFA contribution and actually exceeded the LWFA contribution to the highest-energy electrons in some cases. It was also shown that in the LWFAs studied here, both DLA and LWFA can participate in accelerating the bulk of the electrons in the produced electron beam. The presence of DLA in a LWFA can lead to enhanced betatron oscillation amplitudes and increased divergence in the direction of the laser polarization.

The presence of DLA in LWFA provides insight into possible reasons why the overall quality (i.e., emittance, divergence, energy spread) of the electron beams produced from LWFA experiments is not always competitive with that from conventional radiofrequency accelerators. DLA relies on an exchange of energy between the transverse laser field and the betatron motion of the electrons, which causes the transverse momentum of the electrons to be larger than in a LWFA-only case. This increased transverse momentum can lead to an increase in the transverse size or divergence of the electron beam in the direction of the laser polarization. Additionally, because the energy gain due to DLA varies depending on the magnitude of the transverse laser field sampled by the electron as well as whether or not that electron is able to gain energy from DLA for extended acceleration distances, DLA can contribute to energy spread in LWFA systems such as those studied here. Understanding that DLA can play a role in LWFA systems may provide a path for such experiments to improve the emittance, divergence, and energy spread of their LWFA-produced electron beams if that is a major goal of such experiments.

In the future, the DLA process in LWFA could be developed. One potential path would be to tailor the laser profile to enhance the DLA. For example, the drive laser could be chirped so that the quasi-resonance required for energy gain from DLA is better maintained [8, 9, 11, 13, 14]. The two-laser DLA scheme presented by Zhang *et al* [15, 16] could be tested experimentally to see if it permits better control of the DLA process in LWFA. The effect of ion motion on DLA in a LWFA could be explored through further simulations. Additionally, the gas mix used for ionization injection could be better tailored to trap charge farther forward in the wake. Although such electrons would gain less energy from LWFA, they would overlap with a larger laser amplitude and therefore should gain more energy from DLA. DLA could also be explored in LWFA experiments that utilize other injection methods [6, 49]. Finally, it would be very interesting to investigate whether DLA could be introduced in a beam-driven plasma wakefield accelerator cavity using an intense laser pulse that trails the particle bunch that drives the wake.

DLA also leads to an increase in the amplitude of the betatron oscillations of the electrons. The critical energy of the betatron x-ray spectrum emitted by electrons in a LWFA scales as $\gamma^2 r_0$, where r_0 is the amplitude of the betatron oscillation, and its radiated power scales as $\gamma^2 r_0^2$. The increase in r_0 due to DLA would increase the critical energy and the radiated power. Furthermore, the number of emitted photons scales as $\gamma^{1/2} r_0$ and should therefore increase with the enhanced r_0 from DLA. Therefore, DLA shows much promise as a path to enhancing the betatron radiation generated from LWFAs. In fact, the role of DLA in betatron x-ray production could have been inferred indirectly from the MeV photon emission observed in the forward direction in prior LWFA experiments [50]. The renewed interested in the betatron radiation from LWFAs operating in the self-modulated LWFA regime further motivates additional investigation into the role that DLA plays in betatron radiation [6, 51, 52].

DLA can also be present in LWFA driven by circularly polarized lasers. Additional simulations (not included here) have shown that the presence of two transverse electric field components can lead to continuous energy gain from the DLA mechanism and a correlated increase in the betatron oscillation radius. Furthermore, the degree of polarization of the betatron x-rays produced from circularly polarized DLA-assisted LWFA may be tied to the DLA contribution to the electrons [53].

Finally, DLA could also be applied to microbunch electron beams on femtosecond to attosecond timescales [48]. When DLA is present in a LWFA, the electrons tend to bunch at the extrema of their large-radii betatron oscillations [13, 14]. This bunching is spaced at half of the laser wavelength [8, 13, 14, 48], which can yield electron bunches with temporal durations ~1 fs for a LWFA driven by a Ti:Sapphire laser. It may be possible to diagnose this bunching from the (coherent) optical transition radiation that these bunched beams may emit as they exit the plasma-vacuum boundary.

Acknowledgments

This material is based upon work supported by the Department of Energy National Nuclear Security Administration under Award Number DE-NA0001944, the Department of Energy and National Science Foundation under grant DE-SC0017950, the University of Rochester, and the New York State Energy Research and Development Authority.

The work done at UCLA was supported by US DOE grant DE-SC0010064 and National Science Foundation grant 1734315. NL acknowledges that this work was performed under the auspices of the US Department of Energy by Lawrence Livermore National Laboratory under the contract DE-07NA27344, Lawrence Livermore National Security, LLC. JLS acknowledges use of OSIRIS through the OSIRIS Consortium at UCLA and IST.

This report was prepared as an account of work sponsored by an agency of the US Government. Neither the US Government nor any agency thereof, nor any of their employees, makes any warranty, express or implied, or assumes any legal liability or responsibility for the accuracy, completeness, or usefulness of any information, apparatus, product, or process disclosed, or represents that its use would not infringe privately owned rights. Reference herein to any specific commercial product, process, or service by trade name, trademark, manufacturer, or otherwise does not necessarily constitute or imply its endorsement, recommendation, or favoring by the US Government or any agency thereof. The views and opinions of authors expressed herein do not necessarily state or reflect those of the US Government or any agency thereof.

ORCID iDs

J L Shaw https://orcid.org/0000-0002-1118-8921
N Lemos https://orcid.org/0000-0002-6781-5672

References

[1] Tajima T and Dawson J M 1979 *Phys. Rev. Lett.* **43** 267
[2] Leemans W and Esarey E 2009 *Phys. Today* **62** 3
[3] Cole J M *et al* 2015 *Sci. Rep.* **5** 13244
[4] Kneip S *et al* 2011 *Appl. Phys. Lett.* **99** 093701
[5] Albert F 2015 *Frontiers in Optics 2015 OSA Technical Digest* (San Jose, CA: Optical Society of America) p paper FTh4A.1
[6] Lemos N *et al* 2016 *Plasma Phys. Control. Fusion* **58** 034018
[7] Albert F *et al* 2014 *Plasma Phys. Control. Fusion* **56** 084015
[8] Pukhov A, Sheng Z M and Meyer-ter-Vehn J 1999 *Phys. Plasmas* **6** 2847
[9] Pukhov A 2003 *Rep. Prog. Phys.* **66** 47
[10] Shaw J L, Tsung F S, Vafaei-Najafabadi N, Marsh K A, Lemos N, Mori W B and Joshi C 2014 *Plasma Phys. Control. Fusion* **56** 084006
[11] Shaw J L *et al* 2016 *AIP Conf. Proc.* **1777** 040014
[12] Shaw J L, Lemos N, Marsh K A, Tsung F S, Mori W B and Joshi C 2016 *Plasma Phys. Control. Fusion* **58** 034008
[13] Shaw J L 2016 *PhD Thesis* University of California, Los Angeles
[14] Shaw J L, Lemos N, Amorim L D, Vafaei-Najafabadi N, Marsh K A, Tsung F S, Mori W B and Joshi C 2017 *Phys. Rev. Lett.* **118** 064801
[15] Zhang X, Khudik V N and Shvets G 2015 *Phys. Rev. Lett.* **114** 184801
[16] Zhang X, Khudik V N, Pukhov A and Shvets G 2016 *Plasma Phys. Control. Fusion* **58** 034011
[17] Ralph J E *et al* 2009 *Phys. Rev. Lett.* **102** 175003
[18] Lu W, Tzoufras M, Joshi C, Tsung F S, Mori W B, Vieira J, Fonseca R A and Silva L O 2007 *Phys. Rev. Spec. Top. Accel. Beams* **10** 061301
[19] Wang S *et al* 2002 *Phys. Rev. Lett.* **88** 135004
[20] Rousse A *et al* 2004 *Phys. Rev. Lett.* **93** 135005
[21] Faure J, Rechatin C, Norlin A, Lifschitz A, Glinec Y and Malka V 2006 *Nature* **444** 737
[22] Umstadter D, Kim J K and Dodd E 1996 *Phys. Rev. Lett.* **76** 2073
[23] Esarey E *et al* 1997 *Phys. Rev. Lett.* **79** 2682
[24] Fubiani G, Esarey E, Schroeder C B and Leemans W P 2004 *Phys. Rev.* E **70** 016402
[25] Kotaki H *et al* 2004 *Phys. Plasma* **11** 3296
[26] Faure J *et al* 2009 *C. R. Phys.* **10** 148
[27] Bulanov S, Naumova N, Pegoraro F and Sakai J 1998 *Phys. Rev.* E **58** R5257
[28] Suk H, Barov N, Rosenzweig J B and Esarey E 2001 *Phys. Rev. Lett.* **86** 1011
[29] Chien T Y *et al* 2005 *Phys. Rev. Lett.* **94** 115003
[30] Geddes C G R *et al* 2008 *Phys. Rev. Lett.* **100** 215004
[31] Schmid K *et al* 2010 *Phys. Rev. Spec. Top. Accel. Beams* **13** 091301
[32] Pak A, Marsh K A, Martins S F, Lu W, Mori W B and Joshi C 2010 *Phys. Rev. Lett.* **104** 025003
[33] Oz E *et al* 2007 *Phys. Rev. Lett.* **98** 084801
[34] McGuffey C *et al* 2010 *Phys. Rev. Lett.* **104** 025004
[35] Whittum D H, Sessler A M and Dawson J M 1990 *Phys. Rev. Lett.* **64** 2511
[36] Palmer R B 1972 *J. Appl. Phys.* **43** 3014
[37] Courant E D, Pellegrini C and Zakowicz W 1985 *Phys. Rev.* A **32** 2813
[38] Musumeci P *et al* 2005 *Phys. Rev. Lett.* **94** 154801
[39] Németh K *et al* 2008 *Phys. Rev. Lett.* **100** 095002
[40] Luttikhof M J H, Khachatryan A G, van Goor F A and Boller K J 2010 *Phys. Rev. Lett.* **105** 124801
[41] Nam I *et al* 2011 *Phys. Plasma* **18** 043107
[42] Tochitsky S Y, Williams O B, Musumeci P, Sung C, Haberberger D J, Cook A M, Rosenzweig J B and Joshi C 2009 *Phys. Rev. Spec. Top. Accel. Beams* **12** 050703
[43] Shaw J L, Vafaei-Najafabadi N, Marsh K A and Joshi C 2012 *AIP Conf. Proc.* **1507** 315
[44] Shaw J L 2013 *MS Thesis* University of California, Los Angeles
[45] Mangles S P D *et al* 2006 *Phys. Rev. Lett.* **96** 215001
[46] Fonseca R A *et al* 2002 *Computational Science—ICCS 2002* (*Lecture Notes in Computer Science* vol 2331) ed P M A Sloot *et al* (Berlin: Springer) p 342
[47] Ammosov M V, Delone N B and Krainov V P 1986 *Sov. Phys.-JETP* **64** 1191
[48] Lemos N, Shaw J L, Marsh K A and Joshi C 2016 *AIP Conf. Proc.* **1777** 040009
[49] Kneip S *et al* 2008 *Phys. Rev. Lett.* **100** 105006
[50] Cipiccia S *et al* 2011 *Nat. Phys.* **7** 867
[51] Albert F *et al* 2017 *Phys. Rev. Lett.* **118** 134801
[52] Lemos N *et al* Hyper-spectral directional x-ray source *Phys. Rev. Lett.* to be submitted
[53] Vieira J, Martins J and Sinha U Plasma based helical undulator for controlled emission of circularly and elliptically polarised betatron radiation (arXiv:1601.04422v1 [physics.plasm-ph])